Proceedings of the 45th IEEE Conference on Decision & Control
Manchester Grand Hyatt Hotel
San Diego, CA, USA, December 13-15, 2006

Spacecraft Trajectory Estimation Using a Sampled-Data Extended Kalman Filter with Range-Only Measurements

R. Scott Erwin, Mario A. Santillo, and Dennis S. Bernstein

1. INTRODUCTION

The problem of estimating the full state of a dynamical system based on limited measurements is of extreme importance in many applications. For the case of a linear system with known dynamics, the classical Kalman filter provides an optimal solution [1, 2]. However, state estimation for nonlinear systems remains a problem of research interest.

Besides their value in estimating the state of a system with nonlinear dynamics, nonlinear estimators can also be used to estimate constant states that represent parameters. Consequently, nonlinear filters are useful for system identification [3]. One of the key issues that arises in this application is parameter bias, a longstanding problem [4].

Optimal nonlinear filters have been studied [5], but are often infinite dimensional and thus are difficult to implement. Within a deterministic setting, nonlinear observers have been developed for systems of special structure [6, 7]. Consequently, except for systems of special structure, approximate filters are usually implemented in practice.

There are two main approaches to approximate nonlinear filtering. The first approach is based on a linearization of the nonlinear dynamics and measurement mapping. For example, the extended Kalman filter uses the nonlinear dynamics to propagate the state estimate while using the linearized dynamics and linearized output map to propagate the pseudo-error covariance. The extended Kalman filter is often highly effective, and documented applications cover an extraordinarily broad range of disciplines.

Although the extended Kalman filter was originally conceived within a stochastic setting, recent research has provided a foundation for viewing the extended Kalman filter as a deterministic observer [8–10]. The idea is to adopt or modify the formalisms of the extended Kalman filter while determining conditions that ensure stability and convergence. Although the sufficient conditions are often conservative for specific applications, these results provide an rationalization for the extended Kalman filter formalism

R. Scott Erwin is with the Air Force Research Lab, Space Vehicles Directorate, Kirtland Air Force Base, NM, richard.erwin@kirtland.af.mil

Mario A. Santillo is a graduate student with the Department of Aerospace Engineering, The University of Michigan, Ann Arbor, MI 48109-2140, santillo@umich.edu

Dennis S. Bernstein is with the Department of Aerospace Engineering, The University of Michigan, Ann Arbor, MI 48109-2140, dsbaero@umich.edu

The second approach to approximate nonlinear state estimation foregoes an explicit update of the state estimate error covariance in favor of a collection of filters whose response is used to approximate the state estimate error covariance. These statistical approaches include the particle, unscented, and ensemble Kalman filters [11–13].

The present paper is concerned with state estimation for satellite trajectory estimation, which, for unforced motion, is equivalent to orbit determination [14]. Since orbital dynamics are nonlinear, nonlinear estimation techniques are needed. A wide variety of problems can be considered based on the type of data that are available, including angle (azimuth and elevation), range, and range rate. Range-only orbit determination is considered in [15, 16] which use least-squares approaches and orbital element state representations. The use of angle-only data is considered in [17], which develops a specialized filter to exploit the monotonicity of angles in orbital motion. Issues that arise in the use of range-rate (doppler) measurements are discussed in [18, 19].

Orbit estimation with measurements provided by a constellation of satellites is considered in [20, 21]. One scenario (TDRSS) considers the use of observing satellites in circular, equatorial, geosynchronous orbits to track satellites in low-Earth orbit, while another scenario (GPS) involves the use of a constellation of satellites with pseudo-range measurements (range measurements with clock error biases) to determine the location of the user, but with a significantly different observer-target geometry from the current problem.

In the present paper we consider the use of a constellation of spacecraft in low-Earth orbit to track a satellite in geosynchronous orbit. Since the observing spacecraft have much smaller period than the target satellite in geosynchronous orbit, we must account for blockage by the Earth, and thus the number of available measurements varies with time. We are particularly interested in the ability of the observing spacecraft to acquire and track the target satellite when measurements are available at low frequency, that is, with a large sample interval.

Unlike the study in [20, 21], which considers either angle (two observations per satellite), angle and range (three observations per satellite), and angle, range, and range rate (four observations per satellite), we focus on the case in which only range measurements are available (one obser-

1-4244-0171-2/06/$20.00 ©2006 IEEE.

vation per satellite). In addition, the sample rate in [20] was chosen to be 33 Hz, while we are interested in the ability to track under time-sparse measurements, available on a scale of only minutes or perhaps hours. This constraint is motivated by the need for satellites to simultaneously track a large number of objects.

As in [20, 21], we employ the sampled-data (continuous-discrete) extended Kalman filter [2, p. 188]. This extended Kalman filter involves continuous-time propagation of the state estimate as well as the pseudo-error covariance between measurements and data updates. In practice, the continuous-time state and covariance propagation can be implemented online with high-resolution integration to accurately follow the nonlinear dynamics.

2. Equations of Motion

We consider a single body, called the *target*, orbiting the Earth. We assume a radially symmetric Earth. Except for possible thrusting by the target itself, we ignore all perturbing forces such as drag. The position vector $\vec{r}$ of the target with respect to the center of the Earth satisfies

$$\ddot{\vec{r}} = \frac{-\mu}{r^3}\vec{r} + \vec{w}, \tag{1}$$

where $r \triangleq |\vec{r}|$ is the distance from the satellite to the center of the Earth, $\vec{w}$ denotes forces due to thrusting per unit mass acting on the target, and $\mu \triangleq 398,600$ km^3/s^2 is the Earth's gravitational parameter. The specific thrust $\vec{w}$ is zero unless the target is actively maneuvering.

To cast the dynamics (1) in terms of coordinates, we introduce an inertial reference frame I. It is traditional to choose the inertial reference frame so that the X-axis points toward the Sun on the first day of spring (the vernal equinox line), the Z-axis points through the North pole of the Earth along the axis of rotation, and the Y-axis completes a right-handed coordinate system. This description is approximate since the Earth's rotational axis is not fixed inertially and since the stars move inertially as well [22, pp. 150–153]. However, such details do not play a role in this analysis.

Introducing the velocity vector $\vec{v} \triangleq \dot{\vec{r}}$ and resolving $\vec{r}$, $\vec{v}$, and $\vec{w}$ in I according to

$$\vec{r}\Big|_{\mathrm{I}} = \begin{bmatrix} x \\ y \\ z \end{bmatrix}, \vec{v}\Big|_{\mathrm{I}} = \begin{bmatrix} v_x \\ v_y \\ v_z \end{bmatrix}, \vec{w}\Big|_{\mathrm{I}} = \begin{bmatrix} w_x \\ w_y \\ w_z \end{bmatrix},$$

the equations of motion (1) become

$$\dot{X} = f(X) + W, \tag{2}$$

where

$$X \triangleq \begin{bmatrix} x \\ y \\ z \\ v_x \\ v_y \\ v_z \end{bmatrix}, f(X) \triangleq \begin{bmatrix} v_x \\ v_y \\ v_z \\ -(\mu/r^3)x \\ -(\mu/r^3)y \\ -(\mu/r^3)z \end{bmatrix}, W \triangleq \begin{bmatrix} 0 \\ 0 \\ 0 \\ w_x \\ w_y \\ w_z \end{bmatrix}. \tag{3}$$

Note that $r = \sqrt{x^2 + y^2 + z^2}$.

The vector X provides a complete representation of the target's state, which is characterized by the position and velocity. When the satellite is moving along an orbit, such as a circle, ellipse, parabola, or hyperbola, it is often useful to represent the satellite motion in terms of the six orbital parameters given by the periapsis distance r_{p}, the eccentricity e, the right ascension of the ascending node Ω, the inclination i, the argument of periapsis ω, and the true anomaly ν. The orbital elements r_{p} and e fix the shape of the orbit, while the angles Ω, i, and ω comprise a $(3, 1, 3)$ sequence of Euler rotations that transform the inertial frame to the inertially fixed frame. The true anomaly $\nu(t)$ is a time-dependent parameter that keeps track of the position of the satellite along its orbit. The nonlinear transformations that convert position and velocity into orbital elements and vice versa are given in [22].

3. Measurement Model

For trajectory estimation, we assume that range measurements are available from p satellites at times $t = kh$, where $k = 1, 2, \ldots$. Letting x_i, y_i, z_i denote the inertial coordinates of the ith satellite, assumed to be known accurately, the measurement $Y = Y(kh) \in \mathbb{R}^p$ is given by (omitting the argument kh on the right-hand side)

$$Y(kh) = \begin{bmatrix} d_1(x, y, z, x_1, y_1, z_1) \\ \vdots \\ d_p(x, y, z, x_p, y_p, z_p) \end{bmatrix} + v, \tag{4}$$

where, for $i = 1, \ldots, p$,

$$d_i(x, y, z, x_i, y_i, z_i) \triangleq [(x - x_i)^2 + (y - y_i)^2 + (z - z_i)^2]^{1/2} \tag{5}$$

is the distance from the ith satellite to the target, and $v \in \mathbb{R}^p$ denotes measurement noise.

The measurement d_i is assumed to be unavailable when the line-of-sight path between the ith satellite and the target is blocked by the Earth. To determine blockage, we note that the Earth's surface blocks the path from the ith satellite to the target if and only if there exists $\alpha \in [0, 1]$ such that $D_i(\alpha) < R_{\mathrm{E}}$, where $R_{\mathrm{E}} \triangleq 6378$ km is the radius of the Earth and

$$D_i(\alpha) \triangleq \sqrt{(x_i + \alpha x)^2 + (y_i + \alpha y)^2 + (z_i + \alpha z)^2}.$$

The smallest value of $D_i(\alpha)$ as attained for $\alpha = \alpha_i$, where

$$\alpha_i \triangleq -\frac{x_i x + y_i y + z_i z}{x^2 + y^2 + z^2}.$$

Hence, we compute α_i, ascertain whether α_i lies in the interval $[0, 1]$, and then check the blockage condition $D_i(\alpha_i) < R_{\mathrm{E}}$.

4. Sampled-Data Extended Kalman Filter

Since the equations of motion (1) are nonlinear, we consider an extended Kalman filter. In addition, since we assume that measurements Y are available with a specified sample interval of h sec, we consider a sampled-data extended Kalman filter with data update performed at each time $t = kh$. The sampled-data ("continuous-discrete") extended Kalman filter is given in [2, p. 188]. We use "-" and "+" to denote state estimates before and after data updates, respectively.

4.1. Forecast Step

The forecast (data-free) step of the sampled-data extended Kalman filter consists of the state-estimate propagation

$$\dot{\hat{X}}(t) = f(\hat{X}(t)), \quad t \in [(k-1)h, kh], \tag{6}$$

where

$$\hat{X} \triangleq \begin{bmatrix} \hat{x} & \hat{y} & \hat{z} & \hat{v}_x & \hat{v}_y & \hat{v}_z \end{bmatrix}^{\mathrm{T}}, \tag{7}$$

as well as the pseudo-error covariance propagation

$$\dot{P}(t) = \hat{A}(t)P(t) + P(t)\hat{A}^{\mathrm{T}}(t) + Q, \quad t \in [(k-1)h, kh], \tag{8}$$

where $\hat{A}(t) \triangleq f'(\hat{X}(t))$ is the Jacobian of f evaluated along the trajectory of (6). The Jacobian $\hat{A}(t)$ is given by

$$\hat{A}(t) = \begin{bmatrix} 0_{3\times 3} & I_3 \\ \hat{A}_0(t) & 0_{3\times 3} \end{bmatrix},$$

where (omitting the argument t)

$$A_0(t) \triangleq \mu \begin{bmatrix} \frac{3\hat{x}^2}{\hat{r}^5} - \frac{1}{\hat{r}^3} & \frac{3\hat{x}\hat{y}}{\hat{r}^5} & \frac{3\hat{x}\hat{z}}{\hat{r}^5} \\ \frac{3\hat{x}\hat{y}}{\hat{r}^5} & \frac{3\hat{y}^2}{\hat{r}^5} - \frac{1}{\hat{r}^3} & \frac{3\hat{y}\hat{z}}{\hat{r}^5} \\ \frac{3\hat{x}\hat{z}}{\hat{r}^5} & \frac{3\hat{y}\hat{z}}{\hat{r}^5} & \frac{3\hat{z}^2}{\hat{r}^5} - \frac{1}{\hat{r}^3} \end{bmatrix},$$

where $\hat{r} \triangleq \sqrt{\hat{x}^2 + \hat{y}^2 + \hat{z}^2}$.

Equations (6) and (8) are numerically integrated in real time. Since there is no data injection during the time interval $[(k-1)h, kh]$, variable-step integration can be used for efficiency and accuracy. Let $\hat{X}(kh-)$ and $P(kh-)$ denote the values of $\hat{X}$ and P at the right-hand endpoint of the interval $[(k-1)h, kh]$. At the start of the next interval $[kh, (k+1)h]$, the initial values $\hat{X}(kh+)$ and $P(kh+)$ are determined by the data update step. The overall system is viewed as a sampled-data system in which continuous-time dynamics are interrupted by instantaneous state jumps [23].

4.2. Data Update Step

For the data update step, the linearized measurement map is given by

$$\hat{C}_k \triangleq \begin{bmatrix} \frac{\tilde{x}_1(k)}{\hat{d}_1(k)} & \frac{\tilde{y}_1(k)}{\hat{d}_1(k)} & \frac{\tilde{z}_1(k)}{\hat{d}_1(k)} & 0_{1\times 3} \\ \vdots & \vdots & \vdots & \vdots \\ \frac{\tilde{x}_p(k)}{\hat{d}_p(k)} & \frac{\tilde{y}_p(k)}{\hat{d}_p(k)} & \frac{\tilde{z}_p(k)}{\hat{d}_p(k)} & 0_{1\times 3} \end{bmatrix},$$

where, for $i = 1, \ldots, p$,

$$\tilde{x}_i(k) \triangleq \hat{x}(kh-) - x_i(kh), \quad \tilde{y}_i(k) \triangleq \hat{y}(kh-) - y_i(kh),$$
$$\tilde{z}_i(k) \triangleq \hat{z}(kh-) - z_i(kh),$$
$$\hat{d}_i(k) \triangleq d_i(\hat{x}(kh-), \hat{y}(kh-), \hat{z}(kh-), x_i(kh), y_i(kh), z_i(kh)).$$

Furthermore, the data update gain K_k is given by

$$K_k = P(kh-)\hat{C}_k^{\mathrm{T}}[\hat{C}_k P(kh-)\hat{C}_k^{\mathrm{T}} + R]^{-1}, \tag{9}$$

where Q and R in (8) and (9) are chosen empirically to improve filter convergence. The state-estimate data update is given by

$$\hat{X}(kh+) = \hat{X}(kh-) + K_k[Y(kh) - \hat{d}(k)], \tag{10}$$

where

$$\hat{d}(k) \triangleq [\hat{d}_1(k) \quad \cdots \quad \hat{d}_p(k)]^{\mathrm{T}}.$$

Finally,

$$P(kh+) = (I - K_k\hat{C}_k)P(kh-).$$

The values $\hat{X}(kh+)$ and $P(kh+)$ are used to initialize (6), (8) in the next interval $[kh, (k+1)h]$.

5. Numerical Examples

We consider the case in which satellites in low-Earth orbit (LEO) at a radius of 6600 km are observing a target satellite in an equatorial geosynchronous orbit at a radius of 42,164 km. We assume that the LEO satellites are spaced uniformly around the Earth in an equatorial orbit. With this arrangement, 4 is the smallest number of satellites for which at least 2 satellites are always able to simultaneously view the target. Target tracking with as few as 2 satellites separated by a true anomaly of less than 180 degrees is also possible as long as measurements are guaranteed to be available when the target is in the field of view of both satellites. However, for simplicity, we assume the availability of 4 uniformly spaced LEO satellites with range measurements available (subject to blocking by the Earth) at a fixed sample interval of h sec. All satellite measurements (blocked or not) are assumed to occur simultaneously.

Assuming perfect knowledge of the initial condition and assuming that the target is not maneuvering, it is possible to track the target with arbitrary accuracy without the use of measurements. In practice, perturbing forces such as drag must also be estimated; however, these forces are not considered in this study. When the initial state is unknown or when the target is maneuvering, measurements are needed to track the target. We consider these cases separately.

6. Target Acquisition

We first consider the ability of the sampled-data Kalman filter to acquire the target, that is, to locate the target despite initial position errors. In all cases we set $Q = 0.1 \left[\begin{smallmatrix} 0 & 0 \\ 0 & I_3 \end{smallmatrix}\right]$, and $P_0 = 0$.

We consider gaussian measurement noise with a standard deviation of 0.1 km, which corresponds to $R = 0.01I$ in

(9). For initial estimates that are erroneous by 1 degree and 110 degrees, Figure 1 shows that the position-estimate error reaches a level that is consistent with the measurement accuracy.

Next we consider the ability of the filter to acquire the target under time-sparse measurements with a measurement standard deviation of 0.1 km. For an initial true anomaly error of 10 degrees, Figure 2 shows the position-estimate errors for $h = 1, 10, 50, 100$ sec. In each case, the estimator acquires the target in about 10 data assimilation steps, with ultimate accuracy independent of the sample interval.

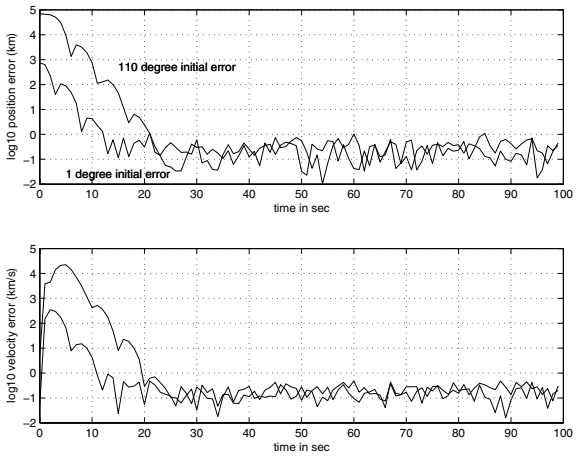

Fig. 1. Target position- and velocity-estimate errors with initial true anomaly errors of 1 degree and 110 degrees. The range data are measured with a sample interval $h = 1$ sec from 4 LEO satellites, and with gaussian measurement noise whose standard deviation is 0.1 km and thus with $R = 0.01I$ in the filter gain expression (9). In both cases the estimator accuracy corresponds to the measurement error level.

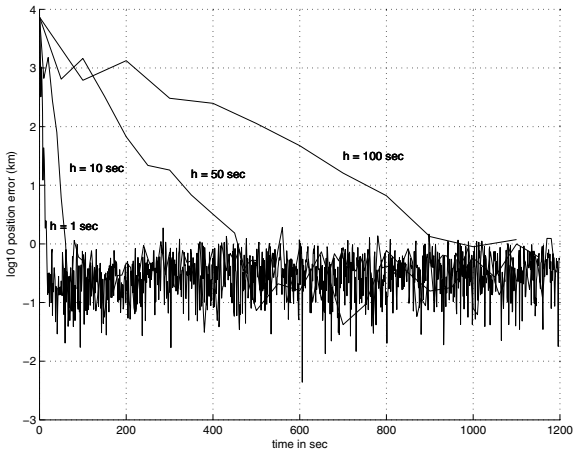

Fig. 2. Target position-estimate error for sample intervals $h = 1, 10, 50, 100$ with range data measured from 4 LEO satellites with a standard deviation of 0.1 km. In each case, the estimator acquires the target in about 10 data assimilation steps, with ultimate accuracy independent of the sample interval.

7. Intermeasurement Tracking Accuracy

Next, we assess the ability of the filter to track the target along its orbit. To see how the position estimate degrades between data updates, we consider an initial true anomaly error of 10 degrees and a sample interval of 50 sec with measurement noise having a standard deviation of 0.1 km. Figure 3 shows the growth of the position error between measurements as well as the position-error reduction that occurs due to data injection.

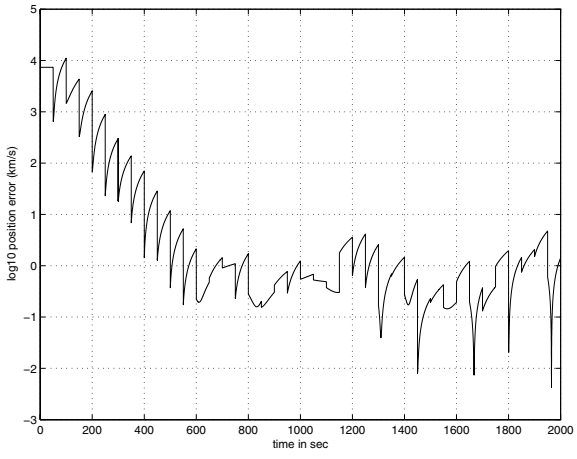

Fig. 3. Target position-estimate error with an initial true anomaly error of 10 degrees, a sample interval of $h = 50$ sec, and a measurement noise standard deviation of 0.1 km. The growth of the position error between measurements can be seen, as well as the position-error reduction that occurs due to data injection.

8. Eccentricity Estimation

We now consider the case in which the target performs an unknown thrust maneuver that changes the eccentricity of its orbit. The initial true anomaly error in all cases is 10 degrees. In particular, the target is initially in a circular orbit as in the previous examples. At time $t = 100$ sec, the target performs a 1-second burn that produces a specific thrust $w = [0\ .5\ 0]^{\mathrm{T}}$ km/s^2, and, at time $t = 200$ sec, the target performs a 1-second burn that produces a specific thrust $w = [0\ .3\ 0]^{\mathrm{T}}$ km/s^2. With an initial eccentricity of $e = 0$, corresponding to the initial circular orbit, the eccentricity after the first burn is $e \approx .35$, while the eccentricity after the second burn is $e \approx .59$. Assuming measurement noise with a standard deviation of 0.01 km and measurements available with a sample interval of $h = 1$ sec, the estimated eccentricity based on the data update estimates is shown in Figure 4. The same scenario is repeated with h increased to 10 sec, with the results shown in Figure 5.

9. Inclination Estimation

We now consider the case in which the target performs an unknown thrust maneuver that changes its inclination. The initial true anomaly error in all cases except where noted is 30 degrees. The target is initially in a circular orbit with inclination $i = 0.1$ rad. At time $t = 100$ sec, the target performs a 1-second burn that produces a specific

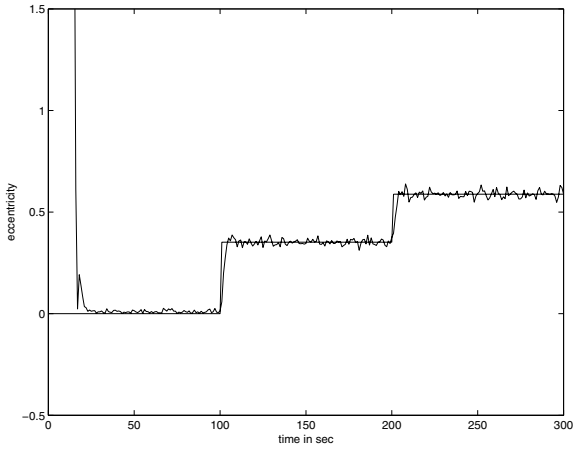

Fig. 4. Estimated eccentricity. The target performs unknown 1-second burns at $t = 100$ sec and $t = 200$ sec. The initial eccentricity is $e = 0$, corresponding to the initial circular orbit, while the eccentricity after the first burn is $e \approx .35$, and the eccentricity after the second burn is $e \approx .59$.

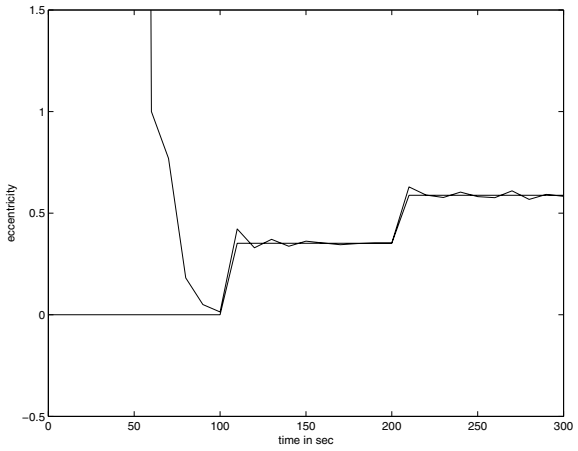

Fig. 5. Estimated eccentricity. This simulation is analogous to Figure 4, where now the sample interval is $h = 10$ sec.

thrust $w = [0\ 0\ .5]^{\mathrm{T}}$ km/s^2, and, at time $t = 200$ sec, the target performs a 1-second burn that produces a specific thrust $w = [0\ 0\ -.2]^{\mathrm{T}}$ km/s^2. The inclination after the first burn is $i \approx 0.26$ rad, while the inclination after the second burn is $i \approx 0.197$ rad. Assuming measurement noise with a standard deviation of 0.01 km and measurements available with a sample interval of $h = 1$ sec, the estimated inclination is shown in Figure 6.

Figure 6 shows that, after a transient, the filter fails to detect the changes in inclination due to the target's maneuvers. This failure suggests that the out-plane-maneuver is due to a lack of observability by the observing satellites in an equatorial orbit.

There are ways to overcome this lack of observability. Initializing the estimated inclination to a small nonzero value results in filter convergence, but if the estimate eventually converges to a zero value, the filter will fail to detect further changes in the target's inclination. Alternatively, we can

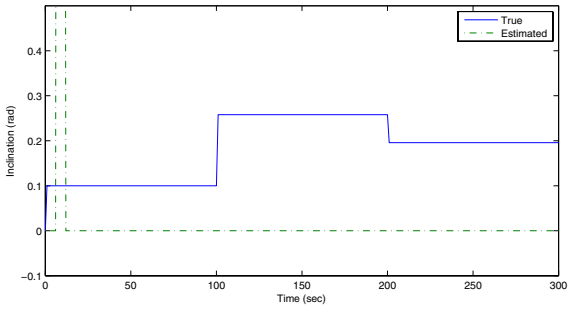

Fig. 6. Estimated inclination. The filter converges to an inclination of 0 rad and fails to detect the changes in inclination due to the target's maneuvers. Further tests suggest a lack of observability by the equatorial observing satellites.

slightly alter the inclination of the observing satellites so that the geometry is not entirely in-plane.

Now, we change the orbit of the first two observing satellites by giving them an inclination of -0.1 rad and -0.2 rad, respectively. After an initial transient, Figure 7 shows the filter's ability to track the true inclination, despite an initial inclination estimate of 0 rad.

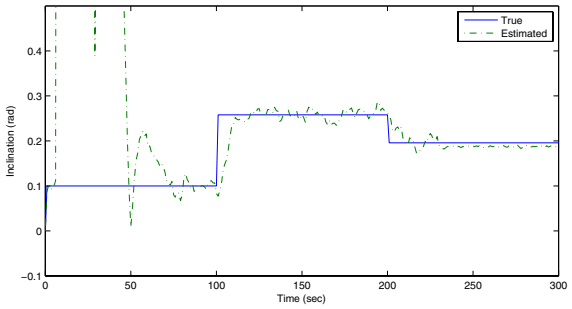

Fig. 7. Estimated inclination. We slightly change the orbit of the first two observing satellites by giving them an inclination of -0.1 rad and -0.2 rad, respectively. After an initial transient, the filter provides improved estimates of the target's inclination.

Finally, we increase the sample interval to $h = 10$ sec. In this case, the filter diverges. However, for an initial true anomaly error of 5 degrees, it can be seen from Figure 8 that the filter can detect changes in the target's inclination.

To explore this observability issue in more detail, consider the undamped mass-spring system with dynamics $\ddot{x}+x = 0$ and measurement given by $y = x^2$. By initializing the estimate at zero, the derivative of y with respect to x evaluated at the initial estimate is also zero; this causes the filter to get "stuck" at this estimate. Figure 9 shows that with a zero initial estimate, the filter does not converge. In contrast, with a small nonzero initial estimate, the filter converges within about 20 sec. In our problem, the out-of-plane range measurement has the same characteristic and thus, the filter fails to converge when the initial estimate is zero and all observing satellites are in an equatorial orbit.

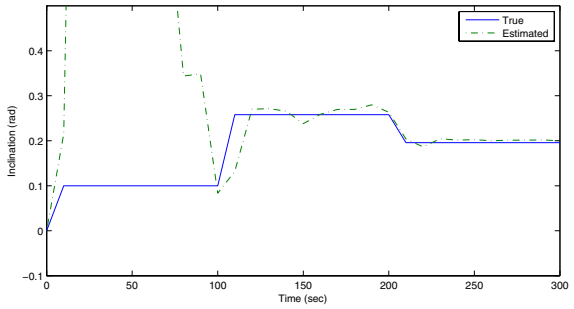

Fig. 8. Estimated inclination. The observing satellite's orbits are as in Figure 7. Now the sample interval is $h = 10$ sec. The filter retains the ability to detect changes in the target's inclination.

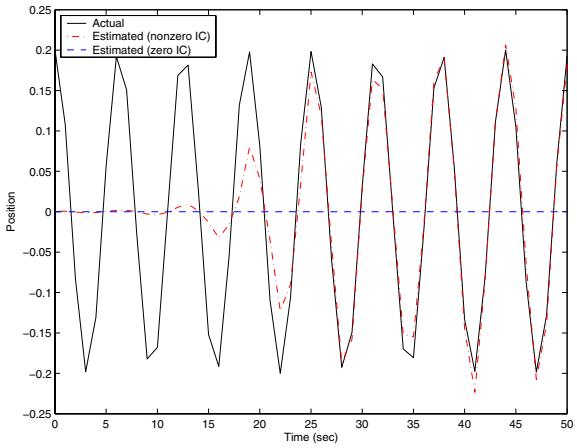

Fig. 9. Example illustrating the extended Kalman filter's failure to converge under special circumstances. Here, the derivative of y with respect to x evaluated at a zero initial estimate is zero, preventing filter convergence. Upon initializing the estimate to a small nonzero value (0.001), the filter converges.

10. Concluding Remarks

Under idealized assumptions on the astrodynamics of bodies orbiting the Earth, we developed a sampled-data extended Kalman filter for range-only observations provided by a constellation of 4 low-Earth orbiting satellites in circular, equatorial orbits. We studied the ability of the filter to acquire and track a target satellite in geosynchronous orbit as a function of the sample interval, initial true anomaly error, and measurement noise standard deviation.

This study complements previous studies that have considered combinations of angle, range, and range-rate measurements by considering range measurements alone and by considering the effects of infrequent measurements.

A surprising discovery of our study is the inability of a constellation of 4 equatorial LEO satellites to track a maneuvering target satellite that changes its inclination when the estimate is identically zero. A simple example illustrated the measurement's characteristics which caused the filter to get "stuck" indefinitely.

The addition of angle (azimuth and elevation) measurements enables the filter to correctly track inclination adjustments when the 4 observing satellites are in an equatorial orbit. Similarly, applying a sampled-data unscented Kalman filter (UKF) to this problem also results in filter convergence. With the UKF, there is no linearized output map to cause the estimate to "stick." Due to lack of space, these extensions are not included here.

References

[1] A. H. Jazwinski, *Stochastic Processes and Filtering Theory*, Academic Press, 1970.

[2] A. Gelb, Ed., *Applied Optimal Estimation*, MIT Press, Cambridge, 1974.

[3] S. K. Sinha and T. Nagaraja, "Extended Kalman Filter Algorithm for Continuous System Parameter Identification," *Comput. Elec. Eng.*, vol. 16, pp. 51–64, 1990.

[4] L. Ljung, "Asymptotic Behavior of the Extended Kalman Filter as a Parameter Estimator for Linear Systems," *IEEE Trans. Autom. Contr.*, vol. AC-24, pp. 36–50, 1979.

[5] F. E. Daum, "Exact Finite-Dimensional Nonlinear Filters," *IEEE Trans. Autom. Contr.*, vol. 31, pp. 616–622, 1986.

[6] A. J. Krener, W. Respondek, "Nonlinear Observers with Linearizable Error dynamics," *SIAM J. Contr. Optim.,* v. 23, 197–216, 1985.

[7] P. E. Moraal and J. W. Grizzle, "Observer Design for Nonlinear Systems with Discrete-Time Measurements," *IEEE Trans. Autom. Contr.*, vol. 40, pp. , 1995.

[8] Y. Song and J. W. Grizzle, "Extended Kalman Filter as a Local Asymptotic Observer for Discrete-time Nonlinear Systems," *J. Math. Sys. Estim. Contr.*, vol. 5, pp. 59–70, 1995.

[9] M. Boutayeb, H. Rafaralahy, and M. Darouach, "Convergence Analysis of the Extended Kalman Filter Used as an Observer for Nonlinear Deterministic Discrete-time Systems," *IEEE Trans. Autom Contr.*, vol. 42, pp. 581–586, 1997.

[10] K. Reif, Konrad and R. Unbehauen, "Extended Kalman Filter as an Exponential Observer for Nonlinear Systems," IEEE Trans. Sig. Proc., vol. 47, pp. 2324–2328, 1999.

[11] S. Julier, J. Uhlmann, and H. F. Durrant-Whyte, "A New Method for the Nonlinear Transformation of Means and Covariances in Filters and Estimators," *IEEE Trans. Autom. Contr.*, v. 45, 477–482, 2000.

[12] F. E. Daum, "Beyond Kalman Filters: Practical Design of Nonlinear Filters," *Proc. SPIE Int. Soc. Opt. Eng.*, v. 2561, 252–262, 1995.

[13] P. L. Houtekamer and H. L. Mitchell, "Data Assimilation Using an Ensemble Kalman Filter Technique," *Monthly Weather Review*, vol. 126, pp. 796-811, 1998.

[14] B. D. Tapley, B. E. Schutz, and G. H. Born, *Statistical Orbit Determination*, Elsevier, Amsterdam, 2004.

[15] N. Duong and C. B. Winn, "Orbit Determination by Range-Only Data," *J. Spacecraft and Rockets*, Vol. 10(2), pp.132-136, 1973.

[16] V. L Pisacane et al., "Orbit Determination from Passive Range Observations," *IEEE Trans. Aerospace and Electronic Sys.*, Vol 10(4), pp. 487-491, 1974.

[17] J. L. Fowler and J. S. Lee, "Extended Kalman Filter in a Dynamic Spherical Coordinate System for Space Based Satellite Tracking," AIAA 23rd Aerospace Sciences Meeting, paper AIAA-85-0289.

[18] D. E. Bizup and D. E. Brown, "Maneuver Detection Using the Radar Range Rate Measurement," *IEEE Trans. Aerosp. Elec. Sys.*, vol. 40, pp. 330–336, 2004.

[19] D. E. Bizup and D. E. Brown,"The Over-Extended Kalman Filter–Don't Use It?," preprint.

[20] D. A. Cicci and G. H. Ballard, "Sensitivity of an Extended Kalman Filter 1. Variation in the Number of Observers and Types of Observations," *Appl. Math. Comput.*, v. 66, 233–246, 1994.

[21] D. A. Cicci, G. H. Ballard, "Sensitivity of an Extended Kalman Filter 2. Variation in the Observation Error Levels, Observation Rates, and Types of Observations," *Appl. Math. Comput.*, v. 66, 247–259, 1994.

[22] H. D. Curtis, *Orbital Mechanics for Engineering Students*, Elsevier, Amsterdam, 2005.

[23] W. Sun, K. Nagpal, M. Krishan, and P. Khargonekar, "Control and Filtering for Sampled-Data Systems," *IEEE Trans. Autom. Contr.*, vol. 38, pp. 1162–1175, 1993.